Molecular basis for SH3 domain regulation of F-BAR–mediated membrane deformation

Yijian Rao[a,1], Qingjun Ma[a,1], Ardeschir Vahedi-Faridi[a], Anna Sundborger[b], Arndt Pechstein[a], Dmytro Puchkov[a], Lin Luo[c], Oleg Shupliakov[b], Wolfram Saenger[a], and Volker Haucke[a,d,e,2]

[a]Institute of Chemistry and Biochemistry, Freie Universität Berlin, 14195 Berlin, Germany; [b]Department of Neuroscience, Linné Center in Developmental Biology and Regenerative Medicine, Karolinska Institutet, 171 77 Stockholm, Sweden; [c]Children's Medical Research Institute, Wentworthville, New South Wales 2145, Australia; [d]Charité Universitätsmedizin Berlin, CC2, 14195 Berlin, Germany; and [e]Leibniz-Institut für Molekulare Pharmakologie, 13125 Berlin, Germany

Communicated by Gottfried Schatz, University of Basel, Reinach, Switzerland, March 18, 2010 (received for review February 2, 2010)

Members of the Bin/amphiphysin/Rvs (BAR) domain protein superfamily are involved in membrane remodeling in various cellular pathways ranging from endocytic vesicle and T-tubule formation to cell migration and neuromorphogenesis. Membrane curvature induction and stabilization are encoded within the BAR or Fer-CIP4 homology-BAR (F-BAR) domains, α-helical coiled coils that dimerize into membrane-binding modules. BAR/F-BAR domain proteins often contain an SH3 domain, which recruits binding partners such as the oligomeric membrane-fissioning GTPase dynamin. How precisely BAR/F-BAR domain-mediated membrane deformation is regulated at the cellular level is unknown. Here we present the crystal structures of full-length syndapin 1 and its F-BAR domain. Our data show that syndapin 1 F-BAR-mediated membrane deformation is subject to autoinhibition by its SH3 domain. Release from the clamped conformation is driven by association of syndapin 1 SH3 with the proline-rich domain of dynamin 1, thereby unlocking its potent membrane-bending activity. We hypothesize that this mechanism might be commonly used to regulate BAR/F-BAR domain-induced membrane deformation and to potentially couple this process to dynamin-mediated fission. Our data thus suggest a structure-based model for SH3-mediated regulation of BAR/F-BAR domain function.

dynamin | endocytosis | membrane bending | syndapin

Eukaryotic cells are characterized by a diverse array of membranous structures including vesicles, tubules, and pleiomorphic vacuoles that enable cellular processes such as organelle biogenesis, cell division, cell migration, secretion, and endocytosis. In most cases, dynamic membrane remodeling is accomplished by the reversible assembly of membrane-deforming proteins (1, 2), most notably by members of the Bin/amphiphysin/Rvs (BAR) domain superfamily (3). BAR domains are characterized by α-helical coiled coils that dimerize into modules with a positively charged surface that interacts with phospholipid membranes (4, 5). Self-assembly of BAR domain proteins, often in combination with the presence of amphipathic helices (6, 7), may then induce or stabilize membrane curvature de novo. Frequently, BAR domain proteins, such as syndapin, sorting nexin 9 (8), endophilin, and amphiphysin (9), also contain an SH3 domain that serves as an interaction platform for proline-rich motif-containing proteins including the large membrane-fissioning GTPase dynamin (10), suggesting that membrane bending is intimately linked with GTP-hydrolysis-dependent vesicle or tubule fission (9, 11, 12). How precisely membrane deformation by BAR domain proteins is regulated at the cellular level and how this may be coupled to fission are largely unknown.

Syndapins [also termed pacsins (13)] are synaptically enriched proteins of the Fer-CIP4 homology-BAR (F-BAR) subfamily of BAR domain proteins that via their SH3 domain bind to dynamin (14) and to actin regulatory proteins such as N-WASP (15) and cordon bleu (COBL) (16). The F-BAR and SH3 domains of syndapins are connected via a flexible linker containing NPF motifs that interact with EH domain proteins, most notably EHD1 (3, 13, 15). Knockdown of syndapin 1 causes impaired axon development and branching and leads to defects in bulk endocytosis of synaptic vesicle (SV) membranes under intense stimulation in primary neurons (17). Similar effects are observed upon perturbation of syndapin function in lamprey reticulospinal axons (18). The role of syndapin in SV recycling appears to be under tight regulatory control by stimulation-induced dephosphorylation of dynamin 1 in nerve terminals (14). Similar regulatory mechanisms must operate to control the membrane-deforming activities of other BAR domain proteins (19–21) and the consumption of membrane buds and tubules by dynamin-mediated fission (9, 12, 17).

Here we show by combined structural, biochemical, and cell biological analysis that syndapin 1 F-BAR-mediated membrane bending is subject to autoinhibition by its SH3 domain. Release from this clamped conformation is driven by association of syndapin 1 SH3 with dynamin 1 or of a proline-rich dynamin 1-derived peptide, thereby unlocking its potent membrane-deforming activity. These data thus suggest a model for SH3-mediated regulation of BAR/F-BAR domain function.

Results

Structural Basis for the Latent Membrane Deformation Activity of Syndapin 1. Syndapin 1 is composed of an N-terminal F-BAR linked to a C-terminal dynamin-binding SH3 domain via a long flexible tether containing NPF motifs (Fig. 1*A*). To analyze its potential membrane-tubulating activity, full-length mouse syndapin 1 fused to eGFP was expressed in Cos7 cells and imaged by live-cell spinning-disk confocal microscopy. Surprisingly, syndapin 1-eGFP displayed a largely cytoplasmic distribution with some enrichment at peripheral plasmalemmal ruffles, but no syndapin 1-coated membrane tubules or vesicles were observed (Fig. 1 *B*, *H*, and *J*). By contrast, expression of syndapin 1 F-BAR-eGFP, a truncation mutant lacking the C-terminal linker-SH3 domain, produced numerous membrane tubules from internal, mostly perinuclear membranes (Fig. 1 *C* and *J*) of an average diameter of about 73 ± 10 nm (Fig. 1*I*) in electron microscopic images. These tubules were accessible to internalized transferrin-Alexa 568 (Fig. S1), suggesting that they were of endosomal origin. A small subfraction of tubules appeared to be plasma membrane-derived. Thus, syndapin 1 harbors a potent membrane-tubulating activity within its F-BAR domain that is suppressed in the full-length protein.

Author contributions: Q.M., O.S., W.S., and V.H. designed research; Y.R., A.V.-F., A.S., A.P., and D.P. performed research; Q.M., L.L., and A.P. contributed new reagents/analytic tools; Y.R., Q.M., A.V.-F., A.S., D.P., O.S., W.S., and V.H. analyzed data; and W.S. and V.H. wrote the paper.

The authors declare no conflict of interest.

Freely available online through the PNAS open access option.

Data deposition: The atomic coordinates and structure factors have been deposited in the Protein Data Bank, www.pdb.org (PDB ID codes 2x3v, 2x3w, and 2x3x).

[1]Y.R. and Q.M. contributed equally to this work.

[2]To whom correspondence should be addressed. E-mail: volker.haucke@fu-berlin.de.

This article contains supporting information online at www.pnas.org/cgi/content/full/1003478107/DCSupplemental.

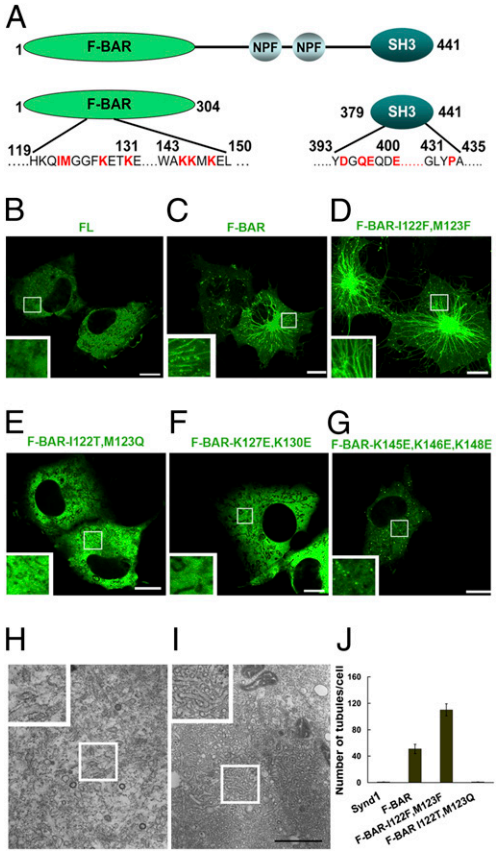

Fig. 1. Syndapin 1 F-BAR but not full-length syndapin 1 forms membrane tubules in living cells. (*A*) Schematic representation of the domain organization of syndapin 1 and of the various truncations and mutants used in this study. (*B*–*G*) Live-cell spinning-disk confocal imaging of Cos7 cells expressing full-length (FL) eGFP-syndapin 1 wild-type or mutants. (*B*) Expression of full-length eGFP-syndapin 1 did not cause membrane tubulation. (*C*–*G*) Membrane tubules induced by expression of eGFP-syndapin 1 F-BAR wild-type (*C*) or (I122F/M123F) (*D*). Mutational inactivation of the amphipathic wedge loop I122T/M123Q (*E*) or the basic belt (K127E/K130E) (*F*) and (K145E/K146E/K148E) (*G*) eliminated the tubulating activity. Representative images from at least three independent experiments are shown. (Scale bars, 10 μm.) (*H* and *I*) Representative electron micrographs of Cos7 cells expressing full-length eGFP-syndapin 1 (*H*) or eGFP-syndapin 1 F-BAR (*I*). Note the presence of numerous F-BAR-induced membrane tubules in *I*. (Scale bar, 0.5 μm.) (*J*) Quantification of the number of eGFP-positive tubules in Cos7 cells expressing syndapin 1 variants. Given are the mean number of tubules (±SE) per cell (n = 3 for each syndapin 1 variant) averaged for at least 20 cells.

To investigate the molecular basis of the membrane-bending activity of syndapin 1 F-BAR, we solved its structure by protein x-ray crystallography using the multiwavelength anomalous diffraction (MAD) method (Table S1). Three F-BAR monomers sit in one crystal asymmetric unit: Two monomers dimerize into an elongated "S" shape with local twofold symmetry (Fig. S2*A*), while the third forms a dimer with its crystal symmetry-related mate. Each monomer consists of four long helices, α1 to α4, and a short C-terminal helix α5 following an extended proline-rich coil (Fig. S2*A*). The head-to-head dimerization of F-BAR domains results in a six-helical bundle consisting of α1, α2, and the N-terminal part of α4 from each monomer and a buried solvent-accessible area of about 4,600 Å^2, indicating a stable dimer in solution. A coiled coil consisting of α3 and the C-terminal part of α4 of each monomer bends to the same side and thus gives the dimer a crescent shape. A striking feature is the charge distribution on the dimer surface: On the concave face, lysines (e.g., K127, K130, K145, K146, K148, K205, and K208) form a continuous positively charged belt, whereas the convex and side surfaces are negatively charged (Fig. S2*D*). The characteristics in scaffold organization and charge distribution are shared with other BAR proteins (3). An interesting feature is that a wedge loop consisting of ^{119}HKQIMGGF^{126}, with hydrophobic residues (I122-M123) at the tip (Fig. S2*B*), protrudes about 12 Å from the area joining α2 and α3. These two helices compose an uninterrupted long helix in other BAR proteins. This wedge loop distinguishes syndapin 1 from known N-BAR and F-BAR proteins. Superposing monomers available in different crystal-packing environments reveals rigidity in the wedge loop (Fig. S2*C*), namely the overall shape and the relative orientation to the helical bundle. Two wedges, with a tip-to-tip distance of about 83 Å in the dimer, are located on the borders of the positively charged concave face and are adjacent to positively charged, conserved residues (e.g., K127 and K130). This may suggest a concerted function of the wedge loop with the charged surface in membrane bending. Two other groups reported similar results regarding the structure of the F-BAR domain from human and *Drosophila* syndapins, respectively (20, 22).

The importance of the wedge loop and the adjacent charged surface for the membrane-tubulating activity of eGFP-F-BAR was confirmed by expression of site-directed mutants (schematically depicted in Fig. 1*A*) in Cos7 cells. Replacing the hydrophobic amino acids I122 and M123 within the wedge loop (Fig. S2*B*) by hydrophilic residues (I122T/M123Q) completely eliminated tubule formation in cells (Fig. 1 *E* and *J*), although this mutation did not alter membrane phospholipid binding. Conversely, mutation of I122 and M123 to phenylalanine, a bulkier hydrophobic residue, significantly increased the number of tubules per cell (Fig. 1 *D* and *J*). Mutational inactivation of either of two basic patches (K127E/K130E or K145E/K146E/K148E) within the positively charged belt on F-BAR abrogated membrane tubulation (Fig. 1 *F*, *G*, and *J*). These data corroborate the structural analysis and confirm the critical role of the positively charged belt and the amphipathic wedge loop in driving syndapin 1 F-BAR-mediated membrane bending.

Crystal Structure of Full-Length Syndapin 1 Reveals an F-BAR-SH3 Clamp. Our own cell-based experiments (Fig. 1) together with recent data using purified syndapin incubated with liposomes (20) suggested that the membrane-tubulating activity of the F-BAR domain is autoinhibited by the SH3 domain. However, the molecular basis for this behavior is not understood. To unravel the structural basis of autoinhibition, we solved the structure of full-length syndapin 1 by protein x-ray crystallography (Fig. 2). We obtained two distinct crystal forms of full-length syndapin 1 (Ful-1, Ful-2) with different unit cell dimensions (Table S1), as confirmed by SDS/PAGE and mass spectrometry. These crystals diffracted x-rays to a maximal resolution of 3.4 and 2.6 Å, respectively (Table S1).

Both Ful-1 and Ful-2 crystals contain one dimer and one monomer of the F-BAR domain in the asymmetric unit, similar to the crystals of the isolated F-BAR domain. In addition, we found extra electron density to fit SH3 domains (385–440). These SH3 domains adopt a conventional β-barrel fold, with the prototyped C-terminal β-strand retrograding to an extended coil (Fig. 2*A*). The RT-src loop and the N-src loop flank the putative PxxP-binding groove with conserved residues such as P434, W420, and Y393 lying at the bottom (Fig. 2*B*). In none of the full-length molecules was the linker connecting the F-BAR and SH3 domains visible, suggesting a high degree of flexibility in this region, in agreement with secondary-structure predictions. Surprisingly, electron density was found for only two SH3 domains in Ful-1 and a single SH3 domain in Ful-2, indicating that physiological interactions can be interrupted by crystal-packing forces. Due to the long invisible linker, it was not possible to assign the SH3 domains to one of the F-BAR domains.

To identify possible physiological interactions between the F-BAR and SH3 domains, the packing of the SH3 domains against the F-BAR domain in the crystal was analyzed. Previous low-resolution data suggested that the SH3 domains of endophilin

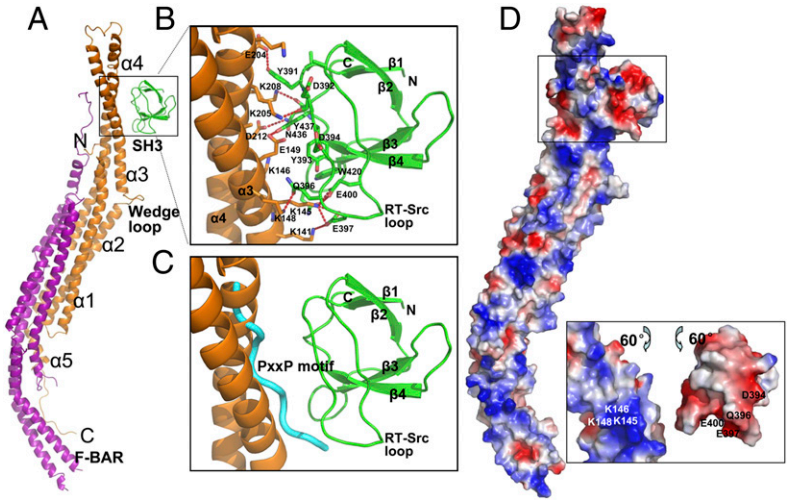

Fig. 2. Structure of full-length syndapin 1. (*A*) Secondary-structure representation of syndapin 1. Protein coloration: gold, chain A; purple, chain B; green, chain D (the SH3 domain). The SH3 domain may be associated with either chain A or chain B of the F-BAR domain, but the lacking electron density for the tether disallows a definite chain assignment. A second SH3 domain found in the asymmetric unit which interacts with the F-BAR domain in an irrelevant manner is not shown in the model. N and C termini, the secondary-structure assignment, and the wedge loop protruding from the long helical region are labeled only on chain A. (*B*) Close-up view of the interface of the SH3 and F-BAR domains. β-Strands of the SH3 domain are labeled. Residues involved in the interaction are shown as a stick model. Polar contacts are presented as red dashed lines. (*C*) A proline-rich peptide (blue) is modeled by hand to the putative PxxP-binding groove in the syndapin 1 SH3 domain, corresponding to the peptide position in the SH3-peptide complex structures PDB ID codes 1W70 and 2DRK. (*D*) The protein surface is colored according to the electrostatic potential: red (negative) through white (neutral) to blue (positive). The lower panel shows an open-up view of the surface charge distribution between F-BAR and SH3. Residues mutated in functional studies are labeled.

(8) and syndapin (20) are placed at or near their respective BAR domains, although the precise position could not be determined. Such an interaction was also found in our crystals (Ful-1), where the SH3 domain with its putative PxxP-binding groove contacts the positively charged concave face at the tip of the F-BAR domain (Fig. 2*A*), with a small buried solvent-accessible area of 460 Å^2. Interestingly, the charge distribution in the SH3 domain is also uneven: negatively charged at the side of the peptide-binding groove and positively charged at the opposite side. Thus, a clear charge complement exists within and near the interface (Fig. 2*D*). Residues at the interface are mainly located in α3 and α4 of the F-BAR domain and the RT-src loop of the SH3 domain. They form an extended hydrogen-bonding and/or salt-bridge network (Fig. 2*B* and Table S2), which is the major contributor to the interaction. In particular, K141, K145, and K148 from α3 of the F-BAR domain intensively interact with Q396, E397, and E400 in the RT-src loop of the SH3 domain. Indeed, ^{145}KKMK^{148} is a common basic motif found in several F-BAR and BAR domain proteins. The interface also contains a small hydrophobic patch formed by aromatic side chains in the peptide-binding groove of the SH3 domain and by aliphatic side chains of the F-BAR domain. The F-BAR/SH3 interaction is mainly mediated by hydrogen bonds/salt bridges, implying that the interaction is salt- and pH-sensitive (see below). The small buried area indicates that the SH3 binds weakly to the F-BAR domain, which is consistent with the observation that SH3 domains generally associate with their binding partners with relatively low affinities (23). However, "complex" formation between the F-BAR and SH3 domains would be significant in solution due to the high local concentration of the two domains within the dimer.

An interaction between the SH3 and F-BAR domains of syndapin 1 is confirmed by direct binding experiments using GST-linker-SH3 or GST-SH3 and His$_6$-F-BAR (Fig. 3*A*). Replacement of K145, K146, and K148 from α3 of the F-BAR with glutamates completely abolished association with GST-SH3 (Fig. 3*B*). Conversely, mutation of the charged/hydrophilic residues D394R/E400R or Q396R/E397R within the RT loop of the SH3 domain also significantly impaired association with the F-BAR domain (Fig. 3*C*), thereby confirming the crystallographically determined interface. To test whether association between the SH3 and F-BAR domains affects membrane tubulation in cells, we cotransfected both domains in trans into Cos7 cells and analyzed these by live-cell spinning-disk confocal microscopy (Fig. S3). Indeed, coexpression of wild-type (WT) mCherry-tagged SH3 strongly impaired the ability of eGFP-F-BAR to generate membrane tubules, whereas SH3s carrying point mutations that interfere with F-BAR association were much less potent (Fig. 3*D*). All SH3-mCherry chimeras were expressed at identical levels (Fig. S3*J*). Hence, the F-BAR and SH3 domains of syndapin 1 interact both in vitro and in living cells.

To assess the specificity of SH3-BAR/F-BAR domain interactions, we analyzed the behavior of the endocytic N-BAR-SH3 domain proteins endophilin 1 and amphiphysin 1. Molecular modeling suggests the existence of a basic patch on the N-BAR domains of endophilin 1 and amphiphysin 1 (Fig. S4) that could serve as a docking site for SH3 domains, in agreement with recent low-resolution small-angle X-ray scattering data (8). To address this possibility, we performed affinity-chromatography experiments using endophilin 1 SH3 or amphiphysin 1 SH3 fused to GST and purified recombinant BAR domains. Both endophilin 1 SH3 (Fig. 3*E*) and amphiphysin 1 SH3 (Fig. 3*F*) bound to their corresponding BAR domains. Interactions between BAR and SH3 domains were also specific to some degree. When offered to different endocytic SH3 domains, syndapin 1 F-BAR preferentially associated with its own SH3 domain, whereas weaker interactions were observed between syndapin 1 F-BAR and amphiphysin 1 SH3 and endophilin 1 SH3 (Fig. 3*G*).

Collectively, the experiments described above suggest that the membrane-tubulating activity of syndapin 1 is under regulatory control by its SH3 domain. The fact that the SH3 contacts the F-BAR domain via its putative PxxP-binding groove further suggests a role for proline-rich SH3 ligands such as dynamin 1 or N-WASP in regulating F-BAR-mediated membrane tubulation. We further explored this putative functional partnership between syndapin 1 and dynamin 1 directly.

Association of Syndapin 1 with Dynamin 1 or a Dynamin 1-Derived SH3-Binding Peptide Unlocks Its Latent Membrane-Tubulating Activity. Our structural analysis indicates that proline-rich SH3 domain ligands

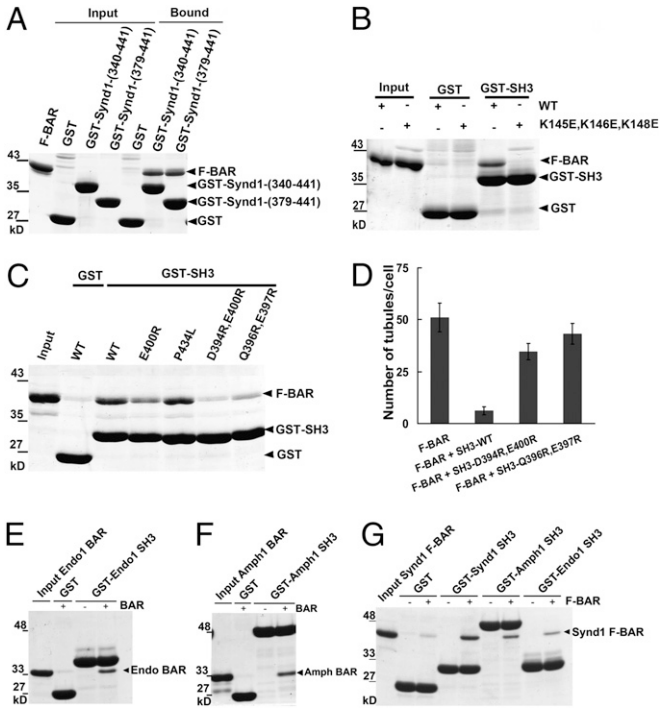

Fig. 3. Complex formation between syndapin 1 F-BAR and SH3 regulates syndapin 1-induced membrane tubulation. (*A*) GST-syndapin 1 SH3 (379–441) or GST-syndapin 1 ΔF-BAR (340–441) bind to their F-BAR domain in vitro, whereas GST does not. (*B*) Mutation of a basic patch on the F-BAR domain (K145E/K146E/K148E) eliminates binding to SH3. (*C*) Mutations within the SH3 domain (D394R/E400R) and (Q396R/E397R) selectively impair binding to the F-BAR domain. By contrast, mutation of the proline-rich motif-binding site on SH3 (P434L) does not affect F-BAR association. Binding assays were done as described in *Materials and Methods*. Samples were analyzed by SDS/PAGE and staining with Coomassie blue. Input, 15% (*A* and *B*) or 10% (*C*) of the total amount of purified F-BAR used for the binding assay. (*D*) Cotransfection of wild-type (WT) but not mutant SH3 inhibits eGFP-syndapin 1 F-BAR-induced membrane tubulation. Shown are the mean number of tubules (±SE) per cell (n = 3 for each syndapin 1 variant) averaged for at least 20 cells. (*E–G*) In vitro binding assays. GST or GST-SH3 fusion proteins were immobilized on glutathione beads and incubated with purified His_6-tagged endophilin 1 BAR (*E*), amphiphysin 1 BAR (*F*), or syndapin 1 F-BAR (*G*) domains. Input, 5% (*E* and *F*) or 3.5% (*G*) of the total amount of purified BAR domains used for the assay. Samples were analyzed by SDS/PAGE and staining with Coomassie blue.

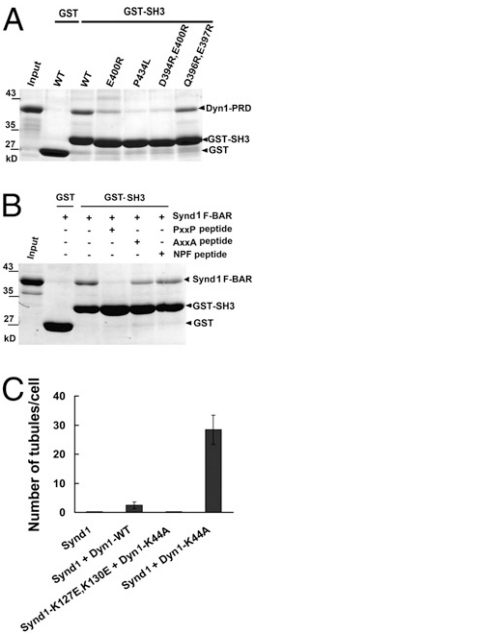

Fig. 4. Association of syndapin 1 SH3 with dynamin 1 releases its tubulating activity from autoinhibition. (*A*) The proline-rich domain of dynamin 1 (Dyn I-PRD) and syndapin 1 F-BAR show partially overlapping binding sites on syndapin 1 SH3. GST pull-down assays were done as described in *Materials and Methods*. (*B*) A dynamin 1-derived syndapin 1-binding wild-type (PxxP) but not an inactive mutant (AxxA) peptide (each at 100 μM) competes with F-BAR for binding to GST-SH3. A peptide derived from the syndapin 1 linker region (NPF) was taken as a further negative control. Samples were analyzed by SDS/PAGE and staining with Coomassie blue. Input, 15% (*A* and *B*) of the total amount of purified F-BAR domain used in the assay. (*C*) Expression of a GTPase-defective dynamin 1 mutant (K44A) unlocks a potent membrane-tubulating activity of eGFP-syndapin 1. Quantification of eGFP-syndapin 1-induced membrane tubules in Cos7 cells coexpressing either mRFP or mRFP-tagged dynamin 1 variants (wild-type or GTPase-defective mutant K44A). Shown are the mean number of tubules (±SE) per cell (n = 3 for each syndapin 1 variant) averaged for at least 20 cells.

such as dynamin 1 may compete with the F-BAR domain for an overlapping surface on the RT loop of SH3 (Fig. 2*C*). Indeed, mutations such as P434L, E400R, or D394R/E400R impair SH3 association with the proline-rich domain (PRD) of dynamin 1 (Fig. 4*A*). By contrast, SH3 Q396R/E397R maintains the ability to bind to dynamin 1 PRD, although it fails to associate with F-BAR (Fig. 3*C*). Hence, dynamin 1 and F-BAR use an overlapping, yet partially distinct interaction surface on the RT loop of the syndapin 1 SH3 domain for binding. This conclusion is further substantiated by peptide competition in direct binding assays. F-BAR domain binding to GST-SH3 is potently inhibited by a dynamin 1-derived proline-rich peptide (PxxP) (14), whereas mutant (AxxA) or unrelated control peptides are inactive (Fig. 4*B*).

If, indeed, association of SH3 with proline-rich ligands releases the F-BAR from the SH3 clamp, addition of a dynamin 1-derived PRD peptide should potently stimulate syndapin 1-mediated membrane bending. We tested this idea using purified syndapin 1 incubated with liposomes in vitro. As expected from our cellular studies, syndapin 1 bound to liposomes (Fig. S5) but did not cause significant tubulation (Fig. 5 *A* and *E*). However, a potent syndapin 1-dependent membrane deformation activity was released upon addition of the dynamin 1 PRD peptide (Fig. 5 *C* and *E*). The dynamin 1 PRD peptide did not alter liposomal membrane association of syndapin 1 (Fig. S5) nor did it cause membrane tubulation on its own. Similarly, breaking the F-BAR-SH3 clamp by mutation (Q396R/E397R) also released the membrane-bending activity of syndapin 1 on liposomes (Fig. 5 *D* and *E*). These results are consistent with a model according to which syndapin 1 functionally cooperates with PRD ligands, most notably dynamin 1, in driving membrane deformation and fission (Fig. 5*F*).

To test such a hypothetical scenario, eGFP-syndapin 1 was coexpressed with either WT or GTP-locked (K44A) dynamin 1-mRFP (Fig. S6 and Fig. 4*C*). Confocal live-cell imaging revealed numerous syndapin 1- and dynamin 1-positive membrane tubules in cells coexpressing eGFP-syndapin 1 and dynamin 1 (K44A)-mRFP (Fig. S6 *D–F* and Fig. 4*C*). Much fewer and shorter tubules were observed in dynamin 1 (WT)-mRFP-transfected cells, which instead accumulated membrane-bound vesicles (Fig. S6 *A–C* and Fig. 4*C*). Membrane tubulation was not observed in cells coexpressing dynamin 1 (K44A)-mRFP together with eGFP-syndapin 1 (K127E/K130E) (Fig. S6 *G–I* and Fig. 4*C*), a variant carrying point mutations within the F-BAR domain that abrogate tubulation (Fig. 1*F*) but do not impair association with either its SH3 domain or with dynamin 1. Conversely, excessive tubulation occurred in cells coexpressing the wedge loop mutant eGFP-syndapin 1 (I122F/M123F), a mutation that enhances tubulation (Fig. 1 *D* and *J*), along with dynamin 1 (K44A)-mRFP (Fig. S7). Tubules

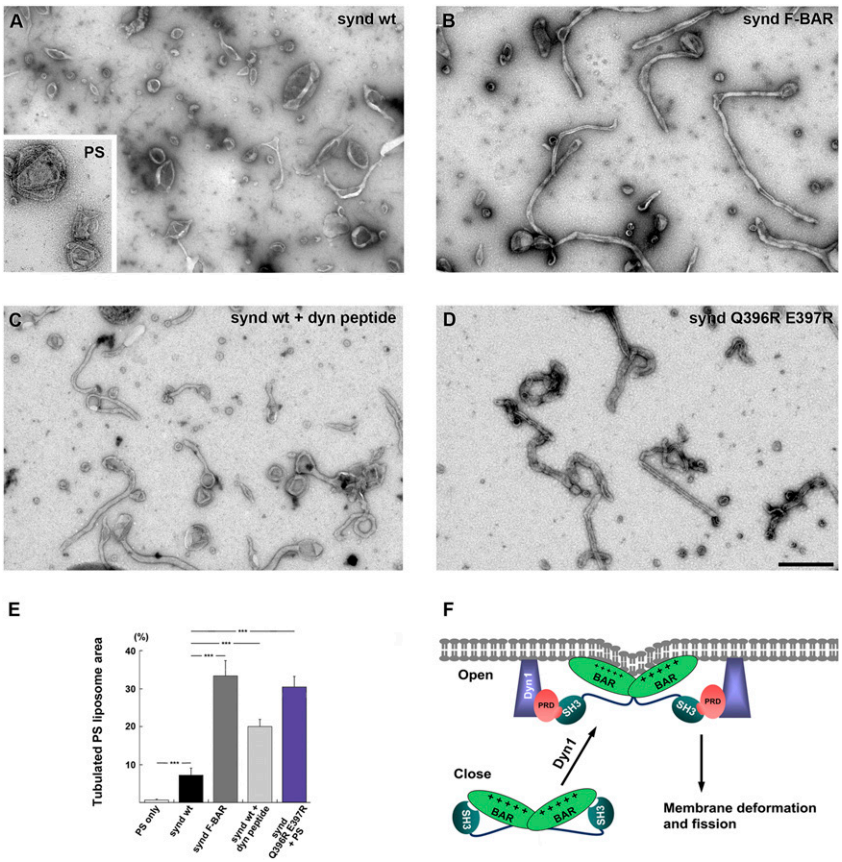

Fig. 5. Syndapin 1-induced membrane tubulation reconstituted on liposomes in vitro. (*A–D*) Negative-stain electron microscopy. (*A*) Transmission electron microscope image of liposomes incubated with full-length (FL) syndapin 1. Inset shows liposomes without the protein. (*B–D*) Representative micrographs of liposomes incubated with syndapin 1 F-BAR (*B*), FL syndapin 1 with 170 μM dynamin peptide (*C*), and FL syndapin 1 (Q396R, E397R) (*D*). (Scale bar, 500 nm.) (*E*) Quantification of liposome tubulation in the experiments illustrated above. Note the significant increase in tubulation efficiency ($P < 0.001$, Student's t test) of FL syndapin 1 after addition of the dynamin peptide or upon mutation of its SH3 domain. (*F*) Hypothetical model for the cooperative role of BAR-SH3 domain-containing proteins and dynamin 1 in membrane deformation and fission. See text for details.

were absent from cells expressing dynamin 1 (K44A)-mRFP (Fig. S6*J* and Fig. 4*C*) or eGFP-syndapin 1 alone (Fig. 4*C*). We conclude that dynamin 1 is able to release the F-BAR domain of syndapin 1 from SH3 domain-mediated autoinhibition, thereby uncovering its latent membrane-deforming activity. Thus, syndapin 1 and dynamin 1 appear to undergo a functional partnership in driving membrane remodeling during endocytosis.

Discussion

BAR domain superfamily proteins play a fundamental role in shaping membranes during diverse cellular processes (3) ranging from the formation of endocytic vesicles (5, 10, 17, 24, 25) and T tubules in muscle (26, 27) to cell migration and morphogenesis (16, 22, 28, 29). Previous studies have allowed us a glimpse at the molecular mechanisms by which BAR/F-BAR domain proteins drive membrane bending (4, 5) or sense and stabilize curved membrane domains (1, 7). A striking feature of many BAR/F-BAR domain proteins is the concomitant presence of at least one SH3 domain (3). In the case of endocytic BAR/F-BAR domain proteins including syndapin, endophilin, and amphiphysin, the SH3 domain acts to recruit proline-rich ligands, most notably the large membrane-deforming and -scissioning GTPase dynamin, a key factor in endocytic membrane fission (10, 11, 30, 31).

In this work, we show that the membrane-deforming activity of syndapin 1, a member of the F-BAR subfamily, is autoinhibited by its SH3 domain. Crystallographic analysis reveals an interaction surface composed of a basic patch on the F-BAR domain that interacts with a corresponding acidic surface on the PRD-binding RT loop of the SH3. Such charge complementarity is also used by PxxP motifs within SH3 domain ligands (32) including dynamin 1.

A somewhat puzzling observation is that SH3 domains appear to bind differently to F-BAR in the crystals. How can this be explained? First, the interaction between the SH3 and F-BAR domains is comparably weak. It is maintained by salt-sensitive charge-charge interactions, and high salt concentrations in the crystallization assay may dissociate SH3 from the F-BAR domain, as seen in direct binding experiments in vitro (Fig. S8). In addition, the syndapin 1 F-BAR domain can assemble into tubules, indicating a noticeable attraction between F-BAR domains. At high concentrations occurring in the crystallization drop, this intermolecular interaction between F-BAR domains may compete with the intramolecular SH3/F-BAR interaction. Hence, SH3 domain positions can be deteriorated by crystal-packing forces.

Physiologically most important, the SH3 clamp on F-BAR is released by complex formation between the syndapin 1 SH3 domain and its binding partner dynamin 1 (14, 17, 24), suggesting a further mechanistic link between F-BAR domain-mediated membrane deformation and fission. Syndapin 1, similar to other BAR-SH3 domain proteins, has been postulated to aid membrane recruitment of dynamin 1 within stimulated nerve terminals (14). Although association of the syndapin 1 F-BAR and SH3 domains suppresses its membrane-deforming activity, phospholipid binding remains largely unaffected.

In a hypothetical scenario, syndapin 1 dimers undergo labile association with membranes (Fig. S5). Capture of dynamin 1 via PRD/SH3 interactions drives several changes: By displacing the SH3 from the F-BAR domain, dynamin 1 facilitates a conformational change within syndapin 1 to the open conformation, thereby releasing the F-BAR domain from geometrical constraints. Self-assembly of dynamin 1 in turn possibly stabilizes syndapin 1 in its membrane-bound state. Reorganization of syndapin 1 F-BAR into a helically arranged lattice, as recently shown for the structurally related proteins CIP4 and FBP17 (4), then serves as a trigger for membrane bending, a process further aided by dynamin 1 coassembly (9, 33) (Fig. 5*F*). Such locally deformed bilayers are then subject to dynamin GTPase-driven fission. It is possible that syn-

dapin 1 directly contributes to this, for example by insertion of the amphipathic wedge loop into one leaflet of the deformed membrane and by stimulating dynamin's GTPase activity. Similar regulatory principles may apply to the role of amphiphysin (10) and endophilin (34, 35) during the fission of late-stage clathrin-coated pits by dynamin during endocytosis or SV recycling. However, additional experimental data are required to test this possibility. Such a model is consistent not only with the data presented here but also with earlier studies (19). A molecularly distinct autoinhibitory mechanism involving the BAR and GAP domains has recently been proposed for members of the GRAF family (21).

SH3-mediated control of BAR/F-BAR domain function may not only be of relevance to endocytic vesicle formation but could be of more general importance. Syndapin family members also are crucial regulators of notochord development (22) and neuromorphogenesis by linking membrane deformation to N-WASP-dependent actin polymerization (28). We speculate that N-WASP binding to syndapin 1 SH3 (15) will cause conformational changes similar to those elicited by association of dynamin. Interestingly, during neuromorphogenesis, syndapin 1 appears to release N-WASP from autoinhibition (28). Hence, syndapin 1 action during actin-dependent remodeling of the neuronal plasma membrane and bulk endocytosis (17) may follow similar regulatory principles.

In summary, we predict that SH3 domain-mediated autoregulation of the membrane-deforming activity of BAR/F-BAR domains is of crucial importance for the function of syndapin 1 and perhaps other BAR domain proteins.

Materials and Methods

SI Materials and Methods include plasmids and peptides; protein purification; crystallization, x-ray data processing and structure solution; transferrin uptake; electron microscopy analysis of protein-lipid tubes; and liposome sedimentation assays.

Protein-Binding Assays. For direct binding assays, immobilized GST fusion proteins (20 μg) were incubated in a total volume of 500 μL in assay buffer (25 mM Hepes, pH 7.0, 50 mM NaCl, and 0.1% Triton X-100) for 2 h at 4 °C with recombinant His_6-tagged proteins (60 or 80 μg) in the presence or absence of peptides (100 μM). Samples were washed extensively. Complexes were analyzed by SDS/PAGE and staining with Coomassie blue. Quantifications were done using ImageJ.

Live-Cell Confocal Imaging Experiments. Cos7 cells expressing low levels of fluorescent proteins were imaged 10–15 h posttransfection with Lipofectamine 2000 (Invitrogen) using a Zeiss Axiovert 200M-based PerkinElmer Life Sciences UltraView ERS dual spinning-disk system. Data were processed using Volocity software (Improvision). For quantification, at least 20 transfected cells were chosen for each experiment. The numbers of tubules were determined and the average number of tubules per cell was calculated. Data from at least three different independent experiments were collected and used for quantification.

Protein Crystallography. Crystals reported here were grown using the hanging-drop vapor-diffusion method. All x-ray diffraction data were collected at the BESSY synchrotron, Berlin, Germany (Table S1). The structure of the syndapin 1 F-BAR domain was solved by the MAD method assisted by a selenomethionine-derived crystal. The full-length syndapin 1 structures were solved by molecular replacement using structures of the refined F-BAR domain and the SH3 domain of Protein Data Bank ID code 2DRK as search models. Detailed procedures are available in *SI Text*. Atomic coordinates and structure factors were deposited in the Protein Data Bank under ID code 2x3v for the structure of the F-BAR domain, and 2x3w and 2x3x for the structures of full-length syndapin 1.

ACKNOWLEDGMENTS. We thank Dr. Oliver Daumke (MDC, Berlin) for critical comments on the manuscript. This work was supported by grants from the Deutsche Forschungsgemeinschaft (Sonderforschungsbereich (SFB) 449/A11 and Forschergruppe (FOR) 806 to V.H.), Swedish Research Council (Projects 13473, 20587), Wallenbergs Foundation and Linné Center (to O.S.), SFB 449/Z3 (to W.S.), Excellence Cluster 257-Neurocure (to V.H.), and the European Science Foundation (to O.S. and V.H.).

1. Hatzakis NS, et al. (2009) How curved membranes recruit amphipathic helices and protein anchoring motifs. *Nat Chem Biol* 5:835–841.
2. Hui E, Johnson CP, Yao J, Dunning FM, Chapman ER (2009) Synaptotagmin-mediated bending of the target membrane is a critical step in Ca(2+)-regulated fusion. *Cell* 138: 709–721.
3. Frost A, Unger VM, De Camilli P (2009) The BAR domain superfamily: Membrane-molding macromolecules. *Cell* 137:191–196.
4. Frost A, et al. (2008) Structural basis of membrane invagination by F-BAR domains. *Cell* 132:807–817.
5. Peter BJ, et al. (2004) BAR domains as sensors of membrane curvature: The amphiphysin BAR structure. *Science* 303:495–499.
6. Itoh T, De Camilli P (2006) BAR, F-BAR (EFC) and ENTH/ANTH domains in the regulation of membrane-cytosol interfaces and membrane curvature. *Biochim Biophys Acta* 1761:897–912.
7. Bhatia VK, et al. (2009) Amphipathic motifs in BAR domains are essential for membrane curvature sensing. *EMBO J* 28:3303–3314.
8. Wang Q, Kaan HY, Hooda RN, Goh SL, Sondermann H (2008) Structure and plasticity of Endophilin and Sorting Nexin 9. *Structure* 16:1574–1587.
9. Takei K, Slepnev VI, Haucke V, De Camilli P (1999) Functional partnership between amphiphysin and dynamin in clathrin-mediated endocytosis. *Nat Cell Biol* 1:33–39.
10. Shupliakov O, et al. (1997) Synaptic vesicle endocytosis impaired by disruption of dynamin-SH3 domain interactions. *Science* 276:259–263.
11. Itoh T, et al. (2005) Dynamin and the actin cytoskeleton cooperatively regulate plasma membrane invagination by BAR and F-BAR proteins. *Dev Cell* 9:791–804.
12. Yoshida Y, et al. (2004) The stimulatory action of amphiphysin on dynamin function is dependent on lipid bilayer curvature. *EMBO J* 23:3483–3491.
13. Modregger J, Ritter B, Witter B, Paulsson M, Plomann M (2000) All three PACSIN isoforms bind to endocytic proteins and inhibit endocytosis. *J Cell Sci* 113:4511–4521.
14. Anggono V, et al. (2006) Syndapin I is the phosphorylation-regulated dynamin I partner in synaptic vesicle endocytosis. *Nat Neurosci* 9:752–760.
15. Kessels MM, Qualmann B (2002) Syndapins integrate N-WASP in receptor-mediated endocytosis. *EMBO J* 21:6083–6094.
16. Ahuja R, et al. (2007) Cordon-bleu is an actin nucleation factor and controls neuronal morphology. *Cell* 131:337–350.
17. Clayton EL, et al. (2009) The phospho-dependent dynamin-syndapin interaction triggers activity-dependent bulk endocytosis of synaptic vesicles. *J Neurosci* 29: 7706–7717.
18. Andersson F, Jakobsson J, Löw P, Shupliakov O, Brodin L (2008) Perturbation of syndapin/PACSIN impairs synaptic vesicle recycling evoked by intense stimulation. *J Neurosci* 28:3925–3933.
19. Farsad K, et al. (2003) A putative role for intramolecular regulatory mechanisms in the adaptor function of amphiphysin in endocytosis. *Neuropharmacology* 45:787–796.
20. Wang Q, et al. (2009) Molecular mechanism of membrane constriction and tubulation mediated by the F-BAR protein Pacsin/Syndapin. *Proc Natl Acad Sci USA* 106: 12700–12705.
21. Eberth A, et al. (2009) A BAR domain-mediated autoinhibitory mechanism for RhoGAPs of the GRAF family. *Biochem J* 417:371–377.
22. Edeling MA, et al. (2009) Structural requirements for PACSIN/Syndapin operation during zebrafish embryonic notochord development. *PLoS One* 4:e8150.
23. Jia CYH, Nie J, Wu CG, Li CJ, Li SSC (2005) Novel Src homology 3 domain-binding motifs identified from proteomic screen of a Pro-rich region. *Mol Cell Proteomics* 4: 1155–1166.
24. Qualmann B, Kessels MM (2002) Endocytosis and the cytoskeleton. *Int Rev Cytol* 220: 93–144.
25. Wieffer M, Maritzen T, Haucke V (2009) SnapShot: Endocytic trafficking. *Cell* 137: 382.e1–382.e3.
26. Kumar V, et al. (2009) Syndapin promotes formation of a postsynaptic membrane system in *Drosophila*. *Mol Biol Cell* 20:2254–2264.
27. Lee E, et al. (2002) Amphiphysin 2 (Bin1) and T-tubule biogenesis in muscle. *Science* 297:1193–1196.
28. Dharmalingam E, et al. (2009) F-BAR proteins of the syndapin family shape the plasma membrane and are crucial for neuromorphogenesis. *J Neurosci* 29:13315–13327.
29. Guerrier S, et al. (2009) The F-BAR domain of srGAP2 induces membrane protrusions required for neuronal migration and morphogenesis. *Cell* 138:990–1004.
30. Bashkirov PV, et al. (2008) GTPase cycle of dynamin is coupled to membrane squeeze and release, leading to spontaneous fission. *Cell* 135:1276–1286.
31. Pucadyil TJ, Schmid SL (2008) Real-time visualization of dynamin-catalyzed membrane fission and vesicle release. *Cell* 135:1263–1275.
32. Zarrinpar A, Bhattacharyya RP, Lim WA (2003) The structure and function of proline recognition domains. *Sci STKE* 2003:RE8.
33. Sweitzer SM, Hinshaw JE (1998) Dynamin undergoes a GTP-dependent conformational change causing vesiculation. *Cell* 93:1021–1029.
34. Verstreken P, et al. (2003) Synaptojanin is recruited by endophilin to promote synaptic vesicle uncoating. *Neuron* 40:733–748.
35. Ringstad N, et al. (1999) Endophilin/SH3p4 is required for the transition from early to late stages in clathrin-mediated synaptic vesicle endocytosis. *Neuron* 24:143–154.